WAVLET-BASED ACTIVE SENSING FOR HEALTH MONITORING OF PLATE STRUCTURES USING BASELINE FREE ULTRASONIC GUIDED WAVE SIGNALS

Sauvik Banerjee*[1], Debadatta Mandal[1], Shaik Mahabu Subhani[1]

[1]Civil Engineering Department, Indian Institute of Technology Bombay,

Powai, Mumbai 400076, India

Emails: sauvik@civil.iitb.ac.in

Submitted: June 24, 2013 ***Accepted: Aug. 3, 2013*** ***Published: Sep. 5, 2013***

Abstract. A wavelet-based active sensing technique for health monitoring of isotropic thin plate-like structures using baseline-free ultrasonic guided Lamb wave signals is presented. In this technique, a built in clock-like piezoelectric (PZT) wafer array of small footprint comprising of a single transmitter and multi-receivers (STMR) is considered. The recorded signals in absence of defects are compared with a theoretical model first, and the velocity and amplitude dispersion of guided waves are studied in an effort to tune an appropriate guided wave mode. A five cycle Hanning pulse is transmitted, and the pulse-echo data recorded at the receivers is processed using two novel algorithms, namely damage index 1 (DI1) and damage index 2 (DI2), based on wavelet transformation to identify defects in the form of cracks and loose rivet holes, which are located both near and far away from the array. In both cases, damage index (DI) maps are generated for identification of defects in a particular coverage area on demand by considering the reflected fundamental guided wave modes. Simulation studies are also

carried out to demonstrate the effectiveness of the proposed sensing technique. The DI maps clearly show higher values of DI at defect locations enabling identification of multiple defects. The DI2 is found to produce better angular resolution of the defect location than the DI1.

Index terms*: ultrasonic guided waves, embedded circular PZT array, wavelet transformation, baseline free algorithms, damage index*

I. INTRODUCTION

Guided wave based structural health monitoring (SHM) approach has shown significant promise in recent years to develop an *in situ* diagnostic imaging system for determining the location and degree of defects in thin plates [1-2] for a number of reasons: (1) it is relatively easy to generate and receive guided waves using piezoelectric transducers located on the surface of the plate; (2) guided waves can propagate a much larger distance than the bulk waves without significant distortion or decay in their shapes with appropriate mode tuning; (3) it is possible to inspect a large area and entire cross-section without the need of expensive motion devices; (4) it is possible to detect different types of damage by utilizing multi modal characteristics of guided waves in metallic [4] or composite [5-8] structures. Usually, anti-symmetric mode tuning is used for surface crack detection, whereas, symmetric mode is tuned for through thickness crack detection [4]. Notably, built-in network of PZT patches has emerged as one of the candidates for continuous and active monitoring of large areas due to low energy consumption, ease of installation in inaccessible areas and great cost-effectiveness [9-11].

Two types of damage diagnosis techniques are reported using built-in PZT patches for active sensing: (a) with baseline (b) without baseline or baseline free. In the former damage detection technique, which is often utilized due to its simplicity, the sensor signals are compared with the base line signals, obtained from the initial condition of the structure. The damage detection algorithm usually involves defining a damage parameter (e.g. damage index) by comparing the changes in extracted signal features at the two states [12-15]. However, it is very difficult to predict defects properly by measuring the changes from the baseline data as in-service structures experience a large variation in their dynamic characteristics due to their exposure to continuously changing environmental conditions (such as temperature variation) as well as changing

operational conditions. So, the changes between the baseline signals and the captured one may be due to the presence of damage or due to the change in environmental and operational conditions. However, efforts have been made to take into consideration the effects of varying environmental conditions, specifically temperature changes, by generating an extensive database of baseline measurements over a range of temperatures [16-18]. To overcome such complications, baseline free damage detection techniques have emerged as a viable alternative. However, literature using these techniques is relatively sparse due their inherent complexity.

The concept of the time reversal method was introduced first by Fink and colleagues for ultrasonic imaging [19, 20] and later adopted for base-line free health monitoring using guided waves [5]. A reference free technique based on instantaneous baseline measurements has been proposed recently by Anton et al [21]. The other method, such as, phased array beam forming [22-24] has been considered as alternatives, however, with some knowledge of the structure in a healthy state, such as group velocity information. These methods deploy 'linear array' of multi-transmitter and multi-receiver (MTMR) and suitably apply weights and time or phase delays to the tapped signals from a sensor array and/or actuator array to obtain the desired directional sensitivities and optimal array gains. A circular array of EMAT transducers based on the concept of MTMR system was also used as Omni-directional guided wave array for inspection of large areas of plate structures [25]. On the contrary, a new compact sensor configuration consisting of a single PZT transmitter and multiple PZT receivers (STMR) as a circular array was considered Rajagopalan et al [26] to ensure uniform coverage and avoid non-uniform insonification associated with beam formation reported for the multi-transmitter multi-receiver (MTMR) system. It was pointed out that this configuration reduces the task of data collection considerably because of the use of single transmitter and that the group velocity information can be instantly obtained and interpolated in all propagation directions. For circular arrays, phased addition algorithm are often used [25, 26] that requires the defect to be in the far-field of the receiver array, so that the reflected wave packets are assumed to come from a particular direction and the signal received at each receiver is shifted appropriately in the wave number domain and added. In contrast, raw time-domain signal data with time of flight and velocity information has been used for damage detection is large plate structures [27]. The STMR array can also be used for detection of plate-stiffener debonding [28].

In this article, the STMR array is considered and two new damage detection algorithms are proposed. The objectives of this research are twofold: a) to study the signal characteristics generated by the commercially available PZT patches based on a theoretical model for appropriate mode tuning, which is essential for damage detection purpose, and b) to develop simplified yet efficient baseline free damage detection algorithms, which are based on wavelet transform of the pulse-echo data to account for both time and frequency domain information. The algorithms rely on the distance of propagation, group velocity and energy or shape of the reflected travelling wave packets without signal shifting. The DI1 is based on the energy content of the reflected fundamental antisymmetric (A_0) or symmetric (S_0) guided wave mode, and DI2 is based on the shape correlation between the excitation signal and the reflected (A_0 or S_0) mode. The advantage of the developed algorithm is that it is capable of inspecting a particular coverage area on demand thereby reducing the task of signal processing. Experiments are performed in a large aluminium plate with multiple defects, such as slits and drilled holes that are placed both at relatively close proximity and far-field of the receiver array. Damage indices (DI1 & DI2) are defined at any point outside the array and index maps are constructed. It is shown that the DI maps exhibits higher values of DI at the defect locations. Numerical studies are also carried out for further validation of the two algorithms.

II. EXPERIMENTAL SET-UP

The test-setup shown in Figure 1 is a National Instruments (NI) PXI platform that consists of an arbitrary signal generator (NI PXI-5412), DAQ card (NI PXI-5105) and a matrix switch (NI PXI-2532). The signal generator is used to generate a tone-burst signal in the form of five-cycle sine pulse modulated with a Hanning window. The DAQ is used to acquire guided wave signals and an external amplifier (Piezo Systems Inc, Model EPA104) is used to achieve adequate signal to noise ratio. The plate considered in this study is of dimension 610mmx610mmx2.5mm and made of Al-5051 aluminum alloy (modulus of elasticity=70GPa, Poisson's ratio=0.33, density =2.68g/cc). The patch type PZT transducers (material type SP-5H) of 10mm dia. and 0.5 mm thickness are used for actuation and sensing. They are bonded to the plate using a commercially available cyanoacrylate based adhesive. A STMR array comprises of PZT patches with 12 receivers (indicated as R) located at 12 equally spaced points on the circumference of a circle and

a transmitter (indicated as S) at the center of the circle, as shown in Figure 2(a). Two types of damage are considered: a) slit of dimension 10 mm x 2mm, and (b) a drilled hole of 5 mm diameter.

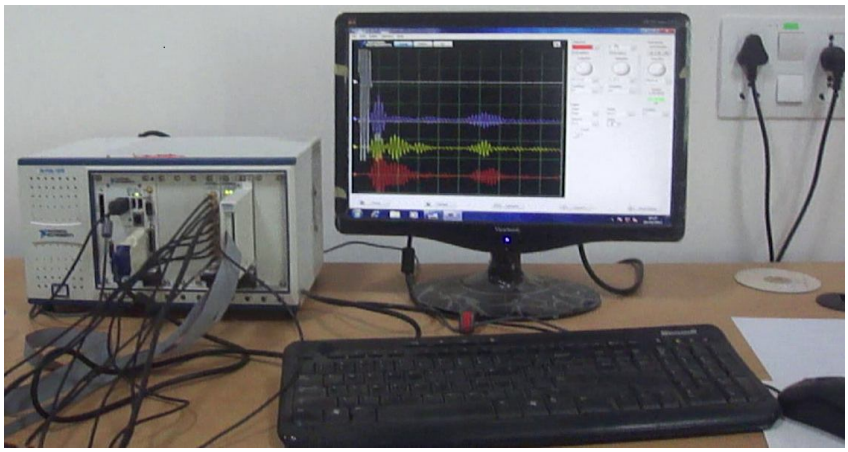

Figure 1. Photograph of the experimental setup consisting of function generator, oscilloscope and computer.

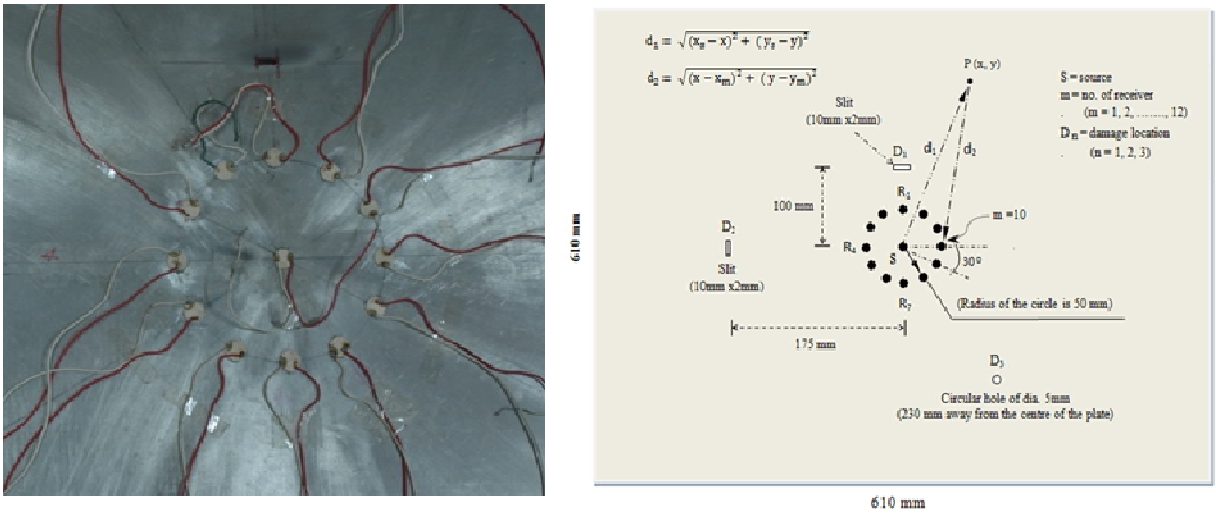

(a) (b)

Figure 2. (a) The experimented aluminum plate showing the arrangements of the PZT patches as STMR array; (b) schematic representation of the plate identifying positions of three defects (D_1, D_2,D_3) with respect to the circular array

Experiments are first performed in an undamaged plate to understand the behavior of the PZT patch and the characteristics of the response signal with the frequency of excitation. Two slits (D_1 and D_2) are then created at two different locations (see Figure 2) and experiments are performed to locate these defects. Then, the hole is drilled far away from the array for further experimentation and validation of the damage detection algorithm. The schematic view of the experimented plate with the locations of the defects with respect to the sensor array is shown in Figure 2 (b).

III. WAVELET TRANSFORMATION

Wave propagation in an elastic medium is the transportation of energy, and the interaction of waves with structural damage and boundary can significantly influence their propagation properties. Wavelet transformation (WT) is a powerful tool of time-frequency analyses of sudden-change signal, accompanying energy reflection, transmission, and mode conversion. Therefore, it is used in many applications in guided waves testing [28-30]. The major advantage of WT is that it retains both the time and frequency domain information of the raw time domain data, thereby, enabling accurate estimation of time of arrival of propagating modes in a wave packet at a particular excitation frequency. All the wavelet transformations (WTs) are calculated with AGU-Vallen Wavelet that uses a Gabor function as the mother wavelet with a central frequency of 7 MHz [31]. AGU-Vallen Wavelet was developed in collaboration between Vallen-Systeme GmbH and Aoyama Gakuin University (AGU), Tokyo, Japan, and has been used extensively in the pioneering research of wavelet analysis in the field of guided wave acoustic emission [32].

IV. DISPERSION CHARACTERISTICS OF GUIDED VAWES

The propagation of Lamb waves is complicated due to two unique features: dispersion and multimode characteristics. Theoretically, these two features can be investigated by solving the Lamb equations defined separately for the symmetrical and anti-symmetrical modes on an infinite isotropic plate with a thickness *d* [33]:

$$\frac{\tanh(\beta d/2)}{\tanh(\alpha d/2)} = -\frac{4\alpha\beta k^2}{(k^2-\beta^2)^2} \tag{1a}$$

$$\frac{\tanh(\beta d/2)}{\tanh(\alpha d/2)} = -\frac{(k^2-\beta^2)^2}{4\alpha\beta k^2} \tag{1b}$$

where,

$$\alpha^2 = \frac{\omega^2}{{c_l}^2} - k^2 \quad and \quad \beta^2 = \frac{\omega^2}{{c_t}^2} - k^2 \tag{1c}$$

where, d = plate thickness, k = wave number = ω/c, c = guided wave phase velocity, c_l = velocities of longitudinal mode, c_t = velocity of transverse mode, ω = wave circular frequency (2πf). For a specific plate made of isotropic material, longitudinal wave velocity (c_l) and shear wave velocity (c_t) are constant as they depend on the material's elastic constants by Rose [33]:

$$c_l = \sqrt{\frac{E}{\rho}\frac{(1-\nu)}{(1+\nu)(1-2\nu)}} \tag{2a}$$

$$c_t = \sqrt{\frac{E}{\rho}\frac{1}{2(1+\nu)}} \tag{2b}$$

The dispersion curves are determined by solving equations (1a) and (1b), and they can be expressed in terms of the product of the excitation frequency and the plate thickness versus the phase velocity (c). For a real ω, c may be either real or complex. A real *c* corresponds to propagating mode in the plate, whereas, a complex *c* corresponds to non-propagating mode that decay exponentially with propagation distance from the source. Thus, for a uniform plate with constant thickness, the dispersion curve can be represented as a function of the frequency. The group velocity (c_g) is given by:

$$c_g = \frac{\Delta\omega}{\Delta k} \tag{3}$$

The group velocity is usually considered to be propagation speed of a wave packet (envelope) with a central frequency carrying maximum energy, whereas, individual frequency component in the packet is propagated at its phase velocity. Thus, it is convenient to use wavelet transformed data of the source and the received signal for the calculation of the group velocity of a propagating mode as follows:

$$c_g = \frac{d}{\Delta t} \tag{4}$$

where, d is the distance between the source (transmitter) and the receiver, and Δt is defined as the time interval between the peaks of the WT envelopes obtained from the source signal and the propagating mode in the received signal, respectively, at the central frequency. The dispersive nature of waves causes the different frequency components of guided waves to travel at different speeds and thus the shape of the wave packet changes as it propagates through a solid medium. The surface response of the plate due to a transient source can be calculated using a wave number integral technique by taking contributions of the propagating modes as described elsewhere Banerjee *et al*. [34] and will not be repeated here.

a. Theoretical and experimental verification

In order to study the dispersion characteristics of guided wave modes, experiments are conducted in a similar undamaged plate with two PZT patches boned at its surface at a spacing 200mm. One of the PZT patches acts as a transmitter and the other as a receiver. Figure 3 illustrates a typical tone-burst signal at a central frequency of 300 kHz given to the PZT transmitter and the associated Fourier transform. The response signal received at the receiver is presented in Figure 4 and compared with that obtained from a theoretical model developed earlier based on wave number integral technique [34]. The model, however, uses an in-plane 'point' excitation and calculates the in-plane surface displacement at 200 mm away from the source, whereas, the PZT patches used in the experiment act on a distributed area and their exact coupling with the plate is unknown. It is seen that the two fundamental guided wave modes, namely, the first anti-symmetric (A_0) and first symmetric (S_0) wave modes are present. S_0 mode is followed by a weak A_0 mode that implies radial vibrations of PZTs. Variations of voltage amplitudes of these two modes with frequencies are presented in Figure 5 for a fixed input voltage of 40Vpp. It is found that S_0 mode provides maximum response at 300kHz. Variations of S_0 and A_0 wave speeds (group velocities) with frequencies are also studied and compared with the theoretical group velocities in Figure 6. Theoretical group velocities are calculated as per Equation (3) and experimental group velocities are calculated using Equation (4). Both the modes are found to be almost non dispersive. Hence, the tone burst signal at 300kHz is considered to be optimal input frequency for further investigations.

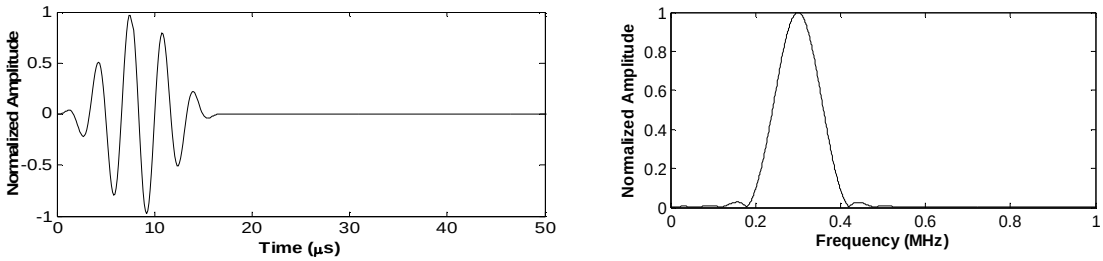

(a) (b)

Figure 3. (a) Excitation signal, and (b) its Fourier spectrum

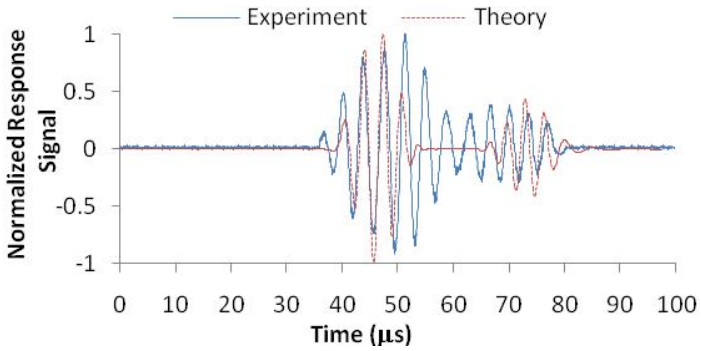

Figure 4. The recorded signal at a distance of 200 mm from the transmitter and its comparison with a theoretical model

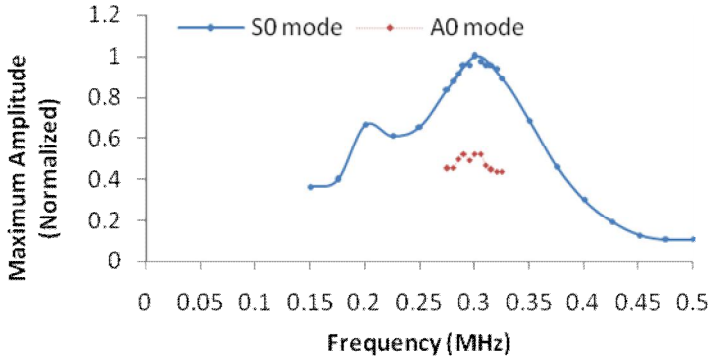

Figure 5. Variations of voltage amplitudes of A_0 and S_0 modes with frequencies

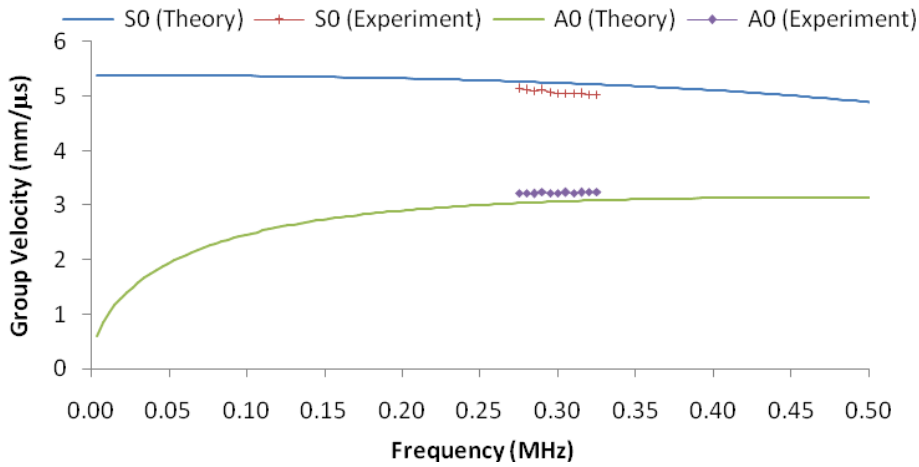

Figure 6. Experimental versus theoretical group velocities of the two modes

V. DAMAGE DETECTION

a. Damage Detection Algorithms

For the purpose of base line free damage detection of the aluminum plate, two detection algorithms have been proposed and developed where a damage index (DI) is defined by taking into account the wavelet transformed data to account for both the time and frequency domain information of the guided wave signals. The transmitter is placed at the center of the aluminum plate and the receivers are arranged at a spacing of 30^0 on the circumference of a circle of radius 50 mm, having the center same as the center of the plate. When the transmitter is excited with a tone-burst signal, guided waves are generated which travel through the plate, guided by free surfaces. If there is any discontinuity in the propagation path of the wave, reflection will occur, resulting in higher values of the Wavelet transform coefficients (WTC) in the received signals. At a central frequency of 300 kHz, the S_0 mode is predominant in experimental investigations, therefore, reflected S_0 mode is tracked for damage detection purpose.

a.i Damage Index 1 (DI1)

Based on the time verses WTC information of received signals, the DI is defined at any point *P(x, y)* on the plate as follows:

$$\mathrm{DI1}(x,y) = \sum_{R=1}^{n} \int_{t_1}^{t_2} (WTC)^2 dt \tag{5}$$

where,

n = number of receivers

WTC = wavelet transform coefficient of the received signal corresponding to the excitation signal frequency at any time

$t_1 = \frac{d_1+d_2}{c_g}$ = time required for the wave to travel from the source to the m^{th} receiver (R_m) via P as in Figure 2

d_1 = distance between the source and the point P

d_2 = distance between the point P and the receiver

c_g = group velocity of the reflected mode (S_0 or A_0)

$t_2 = t_1 + t_s$

t_s = band width of the excitation signal assuming non-dispersive guided wave mode in the response signal

a.ii Damage Index 2 (DI2)

The values of shape norm can vary from -1 to 1, where a value of 1 means perfect correlation and a value of zero means no correlation. Negative values imply that the sense of data is different. The value of shape norms can take any conceivable values depending upon the data. The shape norm is the shape correlation between signals y_i and y_j. It is denoted by ψ_{ij} for correlation between vectors y_i and y_j. and can be used to find a damage index at any point $P(x,y)$ as:

$$DI2 = \psi_{ij} = \frac{\sum_{R=1}^{n} y_i[k]y_j[k]}{(\sum_{R=1}^{n} y_i^2[k])^{1/2}(\sum_{R=1}^{n} y_j^2[k])^{1/2}} \quad (6)$$

Where,

k = range of signal equals to the time bandwidth of the excitation signal

y_i = WTC of the excitation signal, and

y_j = WTC of the received signal.

The time of arrival (t_1) of the reflected signal from any point $P(x,y)$ is same as in DI1. For both the damage indices, it is expected that for a point P, which is very close to the actual damage location, reflected echoes at all receivers create a constructive effect on the damage indices as per Equations (5) and (6).

In the experimental investigation typical signals recorded at receiver numbers 1 (R_1) and 4 (R_4) and their WTC profiles are shown in Figure 7(a)-(b) in the absence and presence of two slits D_1 and D_2. The direct pass and the reflected S_0 modes from the two slits are clearly identified in the

WTC profile. For example, the reflected S_0 mode from slit D_2 arrives at time t_1, and a time bandwidth t_s equals to the time bandwidth of the excitation signal is expected to be retained ignoring the effect of the distributed source (see Figure 7(c)-(d)). However, if the slit is positioned closer to the receiver array, as in the case of D_1, clear separation between the direct pass (combined S_0 and A_0 modes) and the reflected S_0 mode may not be possible. Thus, there is an immediate 'blind coverage area' for inspections both inside and outside the array, that is determined by the footprint (net diameter) of the array and the frequency of the excitation signal. In commercial applications, a size of 3 mm dia PZT patch has been used that can reduce the array footprint drastically [9].

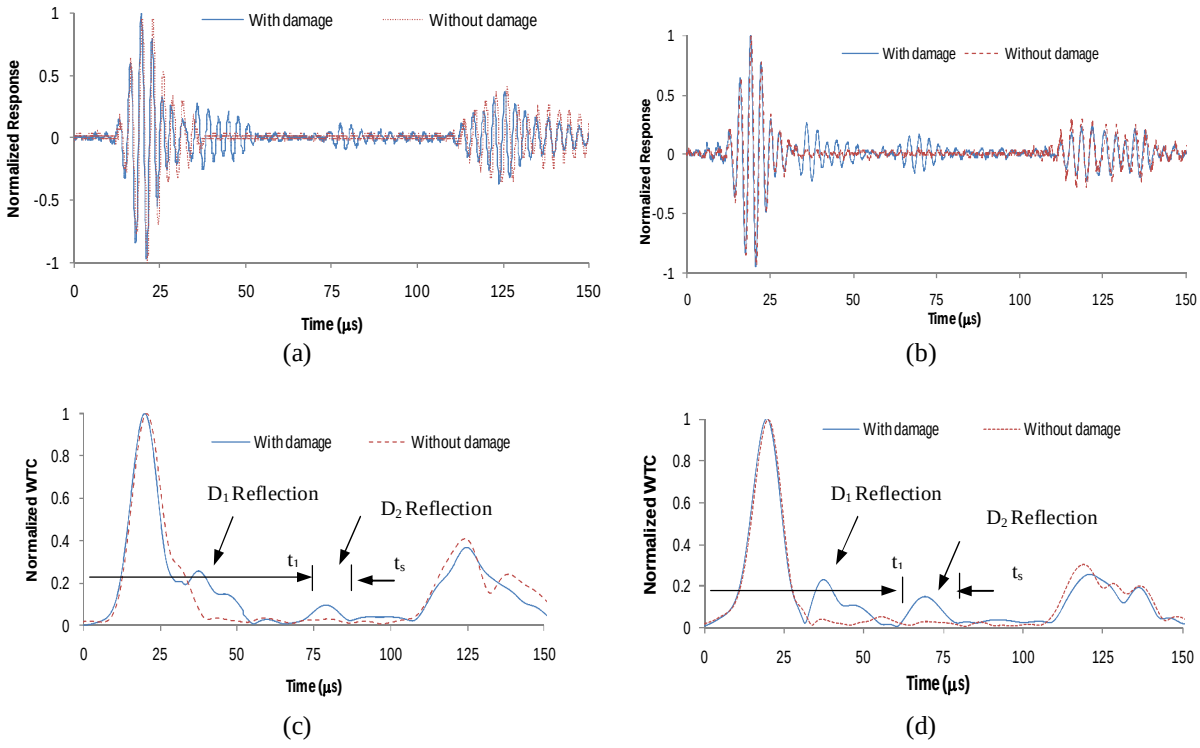

Figure 7. Typical signals recorded with and without the presence of defects D_1 and D_2: (a) response signal at receiver 1 (R_1) ; (b) response signal at receiver 4 (R_4); (c) WTC profile of the response signal at R_1; (d) WTC profile of the response signal at R_4

b. Damage Index Plots

The received signals are processed in two steps: first, wavelet transformation is done on the raw signal data; second, the direct pass and edge reflection are discarded from the wavelet

transformed signal based on the group velocities of the propagating modes. However, edge reflections can be accommodated if the edges of the plate are considered as damage features. Thus, the processed signals are used to calculate DI at different points on the plate. As the dimension of the aluminum plate is 610mmx610mmx2.5mm, a grid of 61x61 node is created to represent the plate in a reduced scale where 1 unit is equivalent to 10 mm. Each node is assumed to be a damage location, P(x,y) and the corresponding DI is calculated as per Eqs. (5) and (6). The algorithms are implemented in MATLAB and the DI maps are plotted in Figure 8. The peak values of DI in the Figure 8(a) and Figure 8(b) indicate the locations of multiple damage (D_1 and D_2) using damage detection algorithms DI1 and DI2, respectively.

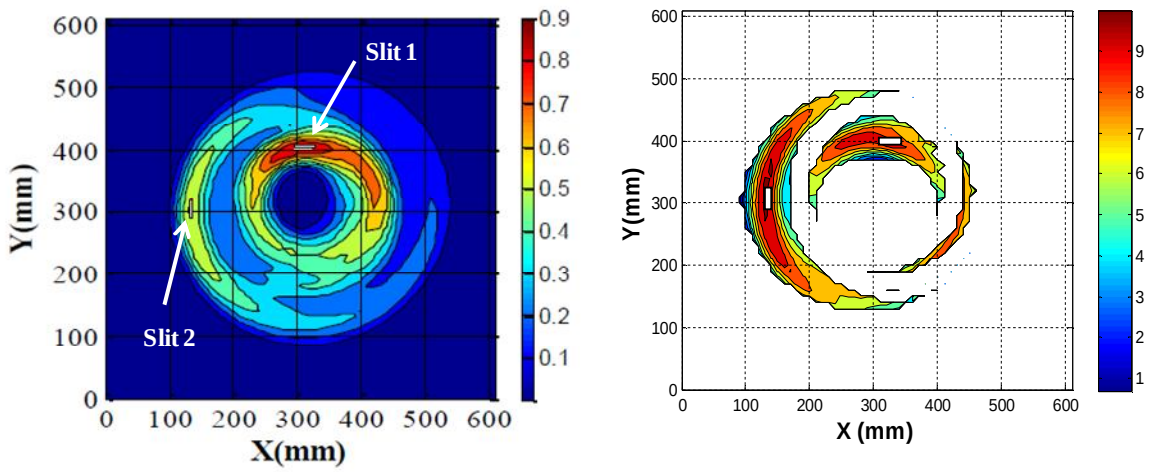

(a) (b)

Figure 8: (a) DI plot of the plate in the presence of D_1 and D_2 using DI1(b) DI plot of the plate in the presence of D_1 and D_2 using DI2. The actual defect locations are marked by white boxes and circles.

The algorithms are capable of inspecting a particular coverage area. As an example, if a coverage area encompassing two radii 150mm and 200mm is considered, then the effect of damage D_1 can be completely eliminated from the DI plots as presented in Figure 9, which only show the presence of damage D_2 located at a distance of 175mm from the transmitter.

Since the defect (D_3) is much smaller involving curved reflecting surface and located at a larger distance compared to the other two defects D_1 and D_2, the echoes captured by the receivers are found to be very weak. Therefore, the input voltage is increased to 60Vpp to achieve an

appropriate signal to noise ratio. Damage index plots in Figure 10 are generated by choosing a coverage area encompassing two radii 200mm and 260mm. It is seen that the DI2 provides better angular resolution of defect location in the damage index map than DI1. The DI plots and the associated contour maps clearly identify the defect locations with a high degree of accuracy.

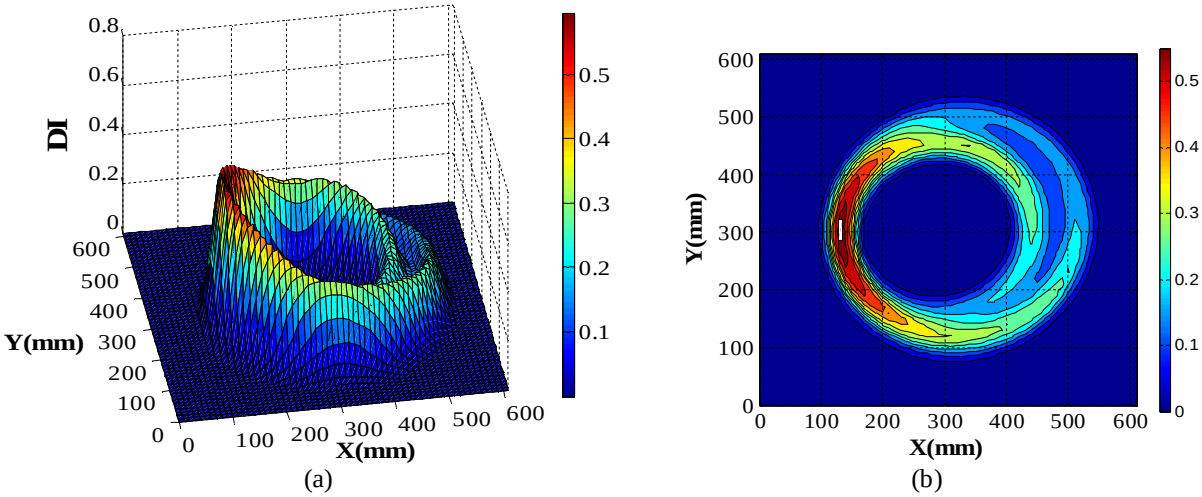

Figure 9. (a) DI plot for a coverage area encompassing two radii 150mm and 200mm showing the highest peak at the defect location D_2 only (b) DI contour map identifying the defect. The actual location of the slit is marked by a white box.

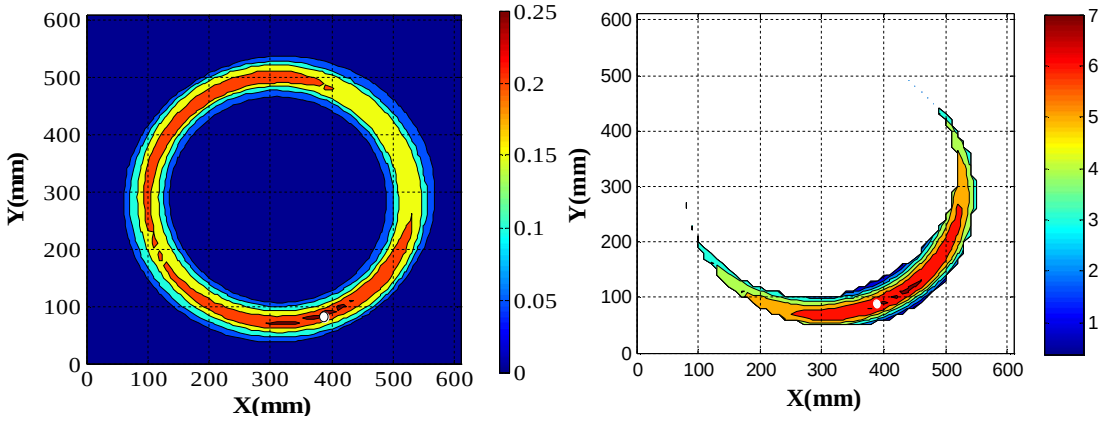

Figure 10. (a) Damage index map (a) using DI1 and (b) using DI2 for a coverage area encompassing two radii 200mm and 260mm showing the highest peak at the defect location D_3 only. The actual location of the 5mm dia hole is marked by a white circle.

VI. SIMULATION STUDIES

The numerical model of the same experimented plate (Figure 2b) with simply support condition is prepared using commercially available finite element package LS-DYNA [35] that utilizes explicit dynamic analysis solver. 8-noded fully integrated brick element is used and the element size is controlled so that its dimension does not exceed one-tenth of the minimum wavelength, which is calculated based on the velocity of the fundamental propagating mode at the excitation frequency. The plate is discretized in 10 elements along the thickness direction, and an element dimension of 1mm is maintained along the planar directions to meet the aforementioned condition in the frequency range of interest. Since the plate is thin, finer discretization is used in the thickness direction to capture the effect of shear deformation appropriately. The meshing around the two types of damage (slit and hole) is shown in Figure 11a.

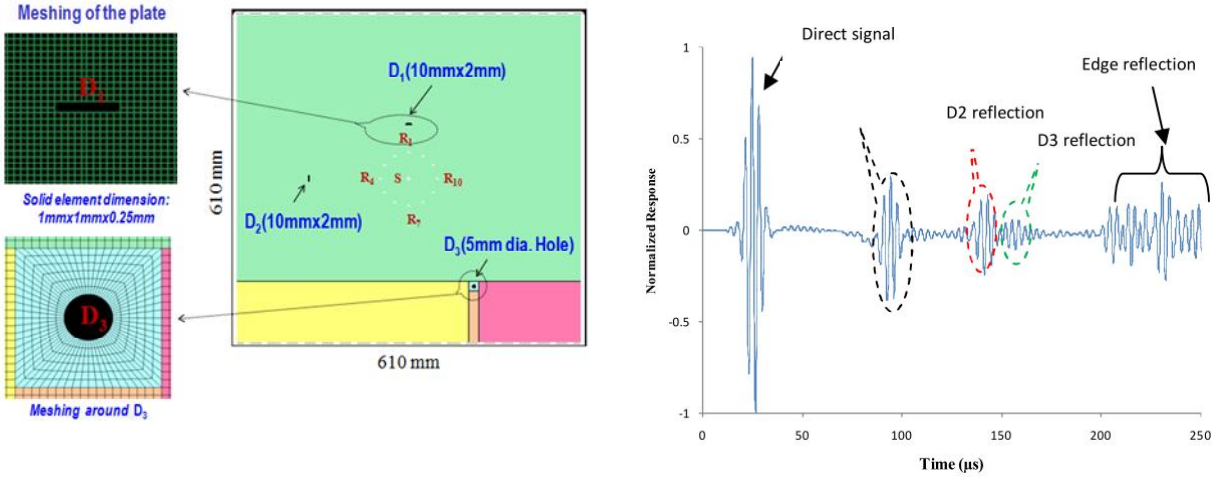

(a) (b)

Figure 11. (a) FE Model of the Aluminum Plate, (b) Typical signal received at receiver R_8. (Normalized)

In the simulation studies, however, A_o mode of vibration of the PZT wafers (or transducers) is considered in order to examine the effectiveness of the two algorithms for A_o mode tracking. It is due to this reason an 'out-of-plane' nodal excitation as in Figure 3(a) is provided at the source (transmitter) location and the 'out-of-plane' nodal surface displacements are calculated at the 12 receiver locations (Figure 2b). A typical simulated signal at receiver no. 8 is shown in Figure 11

(b). The reflected A_o modes from three defects (D_1, D_2, and D_3) can be identified. The received signals are processed in a similar manner as presented in earlier, however, using A0 mode tracking, and the DI maps are plotted in Figure 12 using the two algorithms. The DI maps confirm the presence of three defects with a high degree of accuracy.

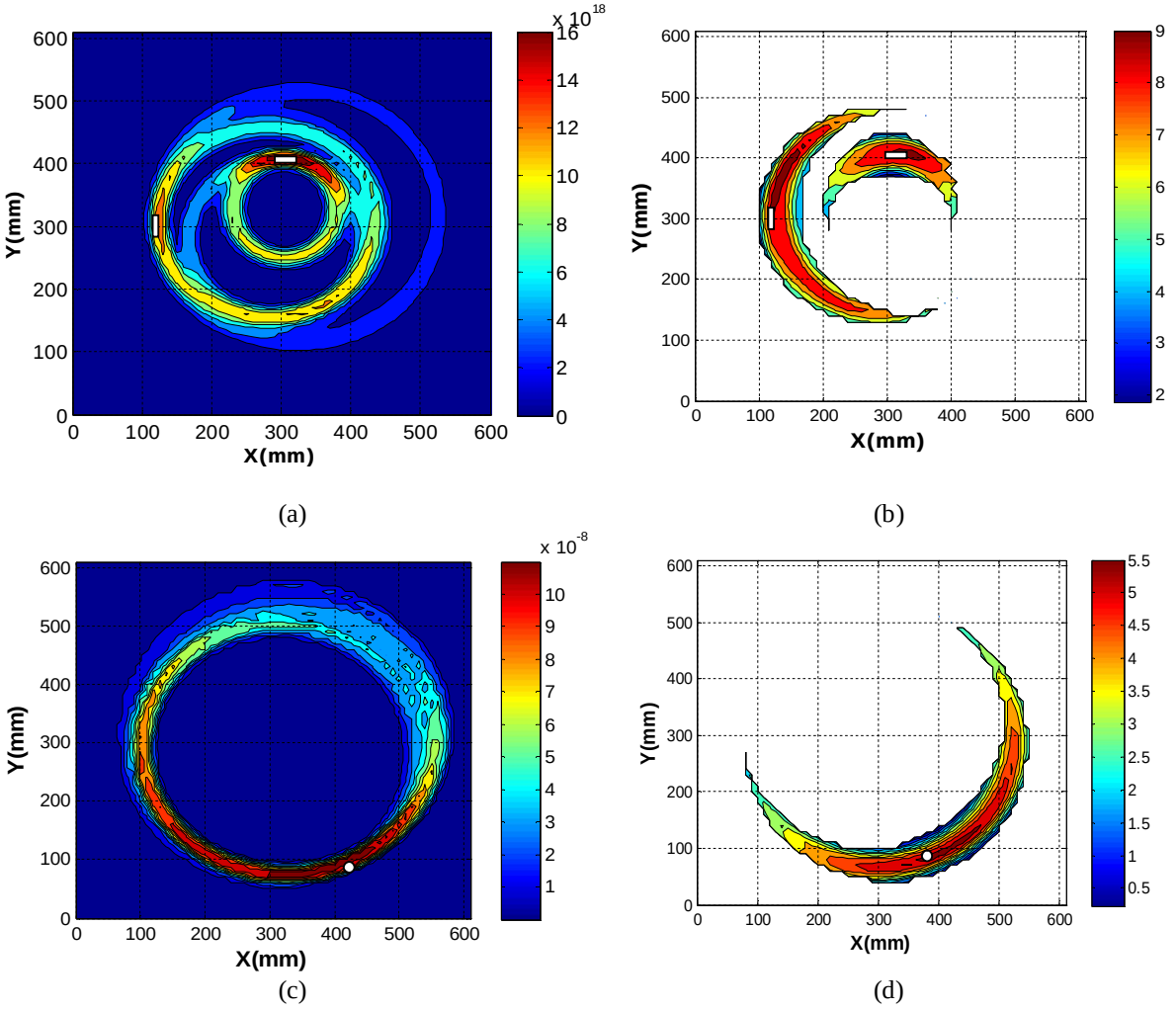

Figure 12. (a) DI plot of the plate in the presence of D_1 and D_2 using DI1(b) DI plot of the plate in the presence of D_1 and D_2 using DI2 (c) DI map showing highest peak at D3 using DI1 (d) DI map showing highest peak at D_3 using DI2. The actual defect locations are marked by white boxes and circles.

VII. CONCLUSIONS

The proposed baseline-free damage detection algorithms based on wavelet transform technique presented in this article are able to locate multiple defects located both at relatively near-field and

far-field of the array with a high degree of accuracy. The DI2 is found to provide superior angular resolution of the defect location in the damage index map compared to DI1. The use of the STMR array as sensors in combination with the wavelet transformation of the signals help in quick and accurate estimation of the group velocities of the propagating modes, thereby eliminating the necessity of other techniques or *a-priori* information on the material properties. The STMR array configuration uses a small footprint of sensors, reduces the task of data collection considerably due to a single transmitter excitation, and allows the group velocity calculations at a number of propagation angles. The behavior of embedded PZT patches and the signal characteristics are studied with the help of a theoretical model. It is found that PZT excites dominating S_0 mode followed by a weak A_0 mode. While the algorithms utilize A_0 or S_0 mode for damage detection purpose, it can, in principle, work even when the received mode is unknown by allowing the algorithm to search through the various modes. Another major advantage of the developed algorithm is that it allows inspection of defects for a selected coverage area that also reduces the time of signal processing.

ACKNOWLEDGEMENT

The research was supported by Indian Space Research Organization under Grant No. 11ISROC001.

REFERENCES

[1] Raghavan, A. and Cesnik, C. E., “Review of guided-wave structural health monitoring”, The Shock and Vibration Digest., Vol. 39, No. 2, pp. 91–114, 2007.

[2] Banerjee, S., Ricci, F., Shih, F. and Mal, A. K., “Structural health monitoring using ultrasonic guided waves”, In Advanced ultrasonic methods for material and structure inspection, T. Kundu (Editor), ISTE, London, U.K. and Newport Beach, CA, USA, Chapter 2, pp. 43-88, 2007.

[3] Chen, J., Su, Z. and Cheng, L., “Identification of corrosion damage in submerged structures using fundamental anti-symmetric Lamb waves”, Smart Materials and Structures, Vol. 19, 015004 (12pp), 2010.

[4] Lingyu, Y. and Cara, A.C.L., "Lamb wave–based quantitative crack detection using a focusing array algorithm", Journal of Intelligent Material Systems and Structures, Vol. 24, No. 9, pp. 1138–1152, 2012.

[5] Park, H. W., Sohn, H., Kincho, H. L. and Farrar, C. R., "Time reversal active sensing for health monitoring of a composite plate", Journal of Sound and Vibration., Vol. 302, pp. 50–66, 2007.

[6] Ramadas, C., Balasubramaniam, K., Joshi, M. and Krishnamurthy, C.V., "Detection of transverse cracks in a composite beam using combined features of Lamb wave and vibration techniques in ANN environment", International Journal on Smart Sensing and Intelligent Systems, Vol.1, No. 4, pp. 970-984, 2008.

[7] Gangadharan, R. , Murthy, C.R.L., Gopalakrishnan, S., Bhat, M. R. and Roy Mahapatra, D., "Characterization of cracks and delaminations using PWAS Lamb waves based time-frequency methods", International Journal on Smart Sensing and Intelligent Systems, Vol. 3, No. 4, pp. 703-735, 2010.

[8] Ben, B.S., Ben, B.A., Vikram, K.A. and Yang, S.H., "Damage identification in composite materials using ultrasonic based Lamb wave method", Measurement, Vol. 46, No. 2, pp. 904–912, 2013.

[9] Giurgiutiu, V., Zagrai, A. and Bao, J. J., "Piezoelectric wafer embedded active sensors for aging aircraft structural health monitoring", Structural Health Monitoring, Vol. 1, No. 1, pp. 41–61, 2002.

[10] Lin, M., Qing, X., Kumar, A. and Beard, S. J., "SMART layer and SMART suitcase for structural health monitoring applications", Proceedings of SPIE: Smart Structures and Materials, Vol. 4332, pp. 98–106, 2001.

[11] Park, J. and Chang, F. K., "Built-in detection of impact damage in multi-layered thick composite structures", In Proceedings of the 4th International Workshop on Structural Health Monitoring, F.K. Chang (Editor), DEStech, Lancaster, pp. 1391-1398, 2003,

[12] Banerjee, S., Ricci, F., Monaco, E. and Mal, A. K., "A wave propagation and vibration-based approach for damage identification in structural components", Journal of Sound and Vibration., Vol. 332, No. 1-2, pp. 167-183, 2009

[13] Monnier, T., "Lamb waves-based impact damage monitoring of a stiffened aircraft panel using piezo-electric transducers", Journal of Intelligent Materials Systems and Structures, Vol. 17, No. 5, pp. 411–421, 2006.

[14] Wang, L. and Yuan, F.G., "Active damage localization technique based on energy propagation of Lamb waves", Smart Structures and Systems., Vol. 3, No. 2, pp. 201-207, 2007.

[15] Nag, C. T. and Veidt, M., "A Lamb-wave based technique for damage detection in composite", Smart Materials and Structures, Vol. 18, 074006 (12pp), 2009.

[16] Lu, Y. and Michaels, J. E., "A methodology for structural health monitoring with diffuse ultrasonic waves in the presence of temperature variations", Ultrasonics, Vol. 43, No. 9, pp. 717– 731, 2005.

[17] Croxford, A. J., Wilcox, P. D., Konstantinidis, G. and B. W. Drinkwater, B. W., "Strategies for overcoming the effect of temperature on guided wave structural health monitoring", Proceedings of SPIE: Health Monitoring of Structural and Biological Systems, Vol. 6532, p. 65321T, 2007.

[18] Sohn, H., "Effects of environmental and operational variability on structural health monitoring", Philosophical Transactions of The. Royal Society of A., Vol. 365, pp 365-539, 2007.

[19] Fink, M., "Time reversal of ultrasonic fields, part I: Basic principles", IEEE Transactions. on Ultrasonics., Ferroelectrics and Frequency Control., Vol. 39, No. 5, pp. 555–566, 1992a.

[20] Fink, M., "Time reversal of ultrasonic fields, part II: Basic principles", IEEE Transactions. on Ultrasonics., Ferroelectrics and Frequency Control., Vol. 39, No. 5, pp. 567–578, 1992b.

[21] Anton, S. R., Inman, D. J. and Park, G., "Reference-free damage detection using instantaneous baseline measurements", The American Institute of Aeronautics and Astronautics Journal**,** Vo. 47, No. 8, 2009.

[22] Giurgiutiu, V. and Cuc, A., "Embedded non-destructive evaluation for structural health monitoring, damage detection, and failure prevention", The Shock and Vibration Digest, Vol. 37, No. 2, pp. 83-105, 2005.

[23] Sundararaman, S., Adams, D. E. and Rigas, E.J., "Structural damage identification in homogeneous and heterogeneous structures using beamforming", Structural Health Monitoring, Vol. 4, No. 2, pp. 171–190, 2005.

[24] Malinowski, P., Wandowski, T., Trendalova. I. and Ostachowicz, W., "A phased array-based method for damage detection and localization in thin plates", Structural Health Monitoring, Vol. 8, No. 1, pp. 5–15, 2005.

[25] Wilcox, P. D., "Omnidirectional guided wave transducer arrays for the rapid inspection of large areas of plate structures", IEEE Transactions. on Ultrasonics., Ferroelectrics and Frequency Control, Vol. 50, No. 6, pp. 699–709, 2003.

[26] Rajagopalan, J., Balasubramaniam, K. and Krishnamurthy, C. V., "A single transmitter multi-receiver (STMR) PZT array for guided ultrasonic wave based structural health monitoring of large isotropic plate structures", Smart Materials and Structures., Vol. 15, No. 5, 1190–1196, 2006.

[27] Kudela, P., Ostachowicz, W. and Zak, A., "Damage detection in composite plates With embedded PZT transducers", Mechanical Systems Signal Processing., Vol. 22, No. 6, pp. 1327–1335, 2008.

[28] Rathod, V. T. and Mahapatra, D. R., "Lamb waves based monitoring of plate-stiffener debonding using a circular array of piezoelectric sensors", International Journal on Smart Sensing and Intelligent Systems, Vol. 3, No. 1, pp. 27-44, 2010.

[29] Bartoli, I., Scalea, F. L. D., Fateh, M. and Viola, E., " Modeling guided wave propagation with application to the long-range defect detection in railroad tracks", NDT&E International, Vol. 38, pp. 325– 334, 2005.

[30] Siqueira, M. H. S., Gatts, C. E. N., da Silva, R. R. and Rebello, J. M. A., "The use of ultrasonic guided waves and wavelets analysis in pipe inspection", Ultrasonics, Vol. 41, pp. 785–797, 2004.

[31] Suzuki, H., Kinjo, T., Hayashi, Y., Takemoto, M. and K. Ono, K., "Wavelet transform of acoustic Emission Signals", Journal of Acoustic Emission., Vol. 14, No. 2, pp. 69-84, 1996.

[32] Hamstad, M. A., A'OGallaghar and Gary, J., "A wavelet transformation applied to acoustic emission signals: Part 1: Source Identification", Journal of Acoustic Emission., Vol. 20, pp. 39-61, 2002.

[33] Rose, J. L., “Ultrasonic waves in solid media”, Cambridge University Press, 1999.

[34] Banerjee, S., Prosser, W. H. and Mal, A. K., “Calculation of the response of a composite plate localized dynamic surface loads using a new wavenumber integral method”, ASME Journal of Applied Mechanics., Vol. 72, No. 1, 18-24, 2005.

[35] LSTC, LS-DYNA Keyword User's Manual, Volume 1, Version 971, Livermore Software Technology Corporation (LSTC), 2007.